

FACULTAD DE INGENIERÍA

Escuela Académico Profesional de Ingeniería Civil

Tesis

Influence of Superstructure Slenderness on the Fragility Curves of Buildings with ADAS, TADAS, and SLB Dissipaters

Abel Max Julcarima Espiritu Angel Ulises Huaman Chuco Jim Alcides Caballero Huaman Manuel Ismael Laurencio Luna

Para optar el Título Profesional de Ingeniero Civil

Huancayo, 2025

Repositorio Institucional Continental Tesis digital



Esta obra está bajo una Licencia "Creative Commons Atribución 4.0 Internacional".

INFORME DE CONFORMIDAD DE ORIGINALIDAD DE TRABAJO DE INVESTIGACIÓN

A : Decano de la Facultad de Ingeniería

DE : Manuel Ismael Laurencio Luna

Asesor de trabajo de investigación

ASUNTO: Remito resultado de evaluación de originalidad de trabajo de investigación

FECHA: 12 de Setiembre de 2025

Con sumo agrado me dirijo a vuestro despacho para informar que, en mi condición de asesor del trabajo de investigación:

Título

Influence of Superstructure Slenderness on the Fragility Curves of Buildings with ADAS, TADAS, and SLB Dissipaters

URL / DOI:

https://www.hrpub.org/download/20250630/CEA13-14841492.pdf / 10.13189/cea.2025.130413

Autores:

- 1. Abel Max Julcarima Espiritu Carrera profesional Ingeniería Civil
- 2. Angel Ulises Huaman Chuco Carrera profesional Ingeniería Civil
- 3. Jim Alcides Caballero Huaman Carrera profesional Ingeniería Civil
- 4. Manuel Ismael Laurencio Luna Carrera profesional Ingeniería Civil

Se procedió con la carga del documento a la plataforma "Turnitin" y se realizó la verificación completa de las coincidencias resaltadas por el software dando por resultado 7 % de similitud sin encontrarse hallazgos relacionados a plagio. Se utilizaron los siguientes filtros:

Filtro de exclusión de bibliografía	SI X	NO
 Filtro de exclusión de grupos de palabras menores Nº de palabras excluidas (en caso de elegir "SI"): 	SI	NO X
Exclusión de fuente por trabajo anterior del mismo estudiante	SI	NO X

En consecuencia, se determina que el trabajo de investigación constituye un documento original al presentar similitud de otros autores (citas) por debajo del porcentaje establecido por la Universidad Continental.

Recae toda responsabilidad del contenido del trabajo de investigación sobre el autor y asesor, en concordancia a los principios expresados en el Reglamento del Registro Nacional de Trabajos conducentes a Grados y Títulos – RENATI y en la normativa de la Universidad Continental.

Atentamente,

La firma del asesor obra en el archivo original (No se muestra en este documento por estar expuesto a publicación)

Civil Engineering and Architecture 13(4): 3001-3019, 2025 http://www.hrpub.org

DOI: 10.13189/cea.2025.130413

Influence of Superstructure Slenderness on the Fragility Curves of Buildings with ADAS, TADAS, and SLB Dissipaters

Abel Max Julcarima Espiritu, Angel Ulises Huaman Chuco, Jim Alcides Caballero Huaman, Manuel Ismael Laurencio Luna*

Faculty of Engineering, Academic School of Civil Engineering, Universidad Continental, Perú

Received March 20, 2025; Revised May 21, 2025; Accepted June 10, 2025

Cite This Paper in the Following Citation Styles

(a): [1] Abel Max Julcarima Espiritu, Angel Ulises Huaman Chuco, Jim Alcides Caballero Huaman, Manuel Ismael Laurencio Luna, "Influence of Superstructure Slenderness on the Fragility Curves of Buildings with ADAS, TADAS, and SLB Dissipaters," Civil Engineering and Architecture, Vol. 13, No. 4, pp. 3001 - 3019, 2025. DOI: 10.13189/cea.2025.130413.

(b): Abel Max Julcarima Espiritu, Angel Ulises Huaman Chuco, Jim Alcides Caballero Huaman, Manuel Ismael Laurencio Luna (2025). Influence of Superstructure Slenderness on the Fragility Curves of Buildings with ADAS, TADAS, and SLB Dissipaters. Civil Engineering and Architecture, 13(4), 3001 - 3019. DOI: 10.13189/cea.2025.130413.

Copyright©2025 by authors, all rights reserved. Authors agree that this article remains permanently open access under the terms of the Creative Commons Attribution License 4.0 International License

Abstract This study evaluates the influence of structural slenderness on the seismic response of buildings equipped with ADAS, TADAS and SLB hysteretic dissipaters. Structures with three levels of slenderness (1, 2 and 3) were modeled and analyzed by means of static and dynamic nonlinear analysis simulations. To quantify structural vulnerability, fragility curves were generated considering Immediate Occupancy, Life Safety and Collapse Prevention performance states as a function of peak ground acceleration (PGA). The results show that the incorporation of dissipaters significantly reduces the inelastic demand and delays the appearance of critical performance states, even in buildings with greater slenderness. However, differences were identified in the effectiveness of each type of dissipator depending on the geometric configuration. In less slender structures, the dissipaters maintained low probabilities of critical damage up to high PGA. On the other hand, in more slender buildings, seismic vulnerability increased significantly above 0.50g, with a higher probability of reaching Life Safety and Collapse Prevention states. The SLB dissipater presented the most uniform performance in all configurations, significantly reducing the probability of severe damage. In contrast, the ADAS and TADAS dissipaters showed a progressive reduction in their damage mitigation capacity as structural flexibility increased, thus

increasing the probability of reaching critical performance states. These findings highlight the importance of adjusting the mechanical properties of dissipaters according to structural slenderness to optimize seismic response. The exploration of advanced strategies, such as the combination of multiple dissipaters and the consideration of geometric variations and soil conditions, is recommended in order to improve structural resilience to large magnitude seismic events.

Keywords Structural Slenderness, Energy Dissipators, Fragility Curves, Seismic Resilience

1. Introduction

The Pacific Ring of Fire is one of the most seismically active regions in the world due to the convergence of tectonic plates, generating earthquakes of a great magnitude that significantly affect populations. Throughout history, several countries located in this area have suffered devastating events that highlight the vulnerability of infrastructures and underscore the implementing importance of effective preparedness strategies. For example, recently, on April 3, 2024, Taiwan experienced an earthquake of magnitude Mw 7.4 that left at least 500 injured, being considered the most intense in the last 25 years [1]. Likewise, Ecuador faced on April 16, 2016 an earthquake of magnitude Mw 7.8 with more than 900 fatalities and approximately 6,000 injured, in addition to thousands of victims [2]. These events reinforce the need to promote mitigation and resilience measures in the face of large magnitude earthquakes.

Peru, also located in this region of high seismic activity [3], recorded the last major earthquake on its central coast in 1746 with an estimated magnitude between Mw 8.8 and Mw 9 [4]. More recently, the 2007 Pisco earthquake with a magnitude of Mw 7.9 caused 596 deaths, more than 431,000 victims and generated a moderate tsunami [5]. Currently, the coastline that encompasses Lima is going through a seismic silence of more than 278 years, due in 2024, which indicates the possibility of seismic energy being released at any time by a large magnitude earthquake [4].

Recent studies on seismicity and cortical deformation in the Peruvian western edge point to a marked accumulation of stresses off the coasts of Lima-Callao, Moquegua and Tacna, indicating a high potential for large magnitude earthquakes. Likewise, the identification of seismic gaps and zones of maximum coupling suggests possible events of up to Mw 8.8 in Lima-Callao, Mw 7.9 in Ica-Arequipa and Mw 8.2 in Moquegua-Tacna. Specifically, an earthquake of magnitude Mw 8.8 in Metropolitan Lima could generate shaking greater than 500 cm/s ? representing a very significant risk [6].

In the face of this threat, it is crucial that buildings guarantee the safety of people and minimize structural damage [7]. Traditional seismic-resistant design based mainly on shear walls or reinforced concrete frames may be insufficient for high intensity earthquakes and, in some cases, increase costs without guaranteeing comprehensive protection. In this context, energy dissipation devices emerge as an effective alternative to reduce the seismic demand, since they allow dissipating the energy and reducing the internal forces in the structure [8].

In Chile, a study on the optimization of hysteretic dissipaters in reinforced concrete frames of 5, 10 and 15 stories showed remarkable reductions in displacements and improvements in the global resistance, although absolute accelerations did not decrease. Likewise, in taller and slender structures, it was necessary to use less rigid dissipators with lower creep forces to maximize efficiency [9]. However, it is still not clearly understood how the slenderness of the superstructure influences the fragility curves, which are fundamental to estimate the probability of damage at different levels of seismic intensity.

Therefore, this study examines the relationship between superstructure slenderness and fragility curves in buildings equipped with ADAS, TADAS and SLB dissipaters. Understanding how structural features modify seismic response will allow for more efficient design and strengthening of buildings. Evaluating the effectiveness of these devices and their proper integration into the structural design is essential to mitigate risks and safeguard the lives of occupants.

2. Literature Review

In Peru, the incorporation of energy dissipaters to protect buildings against earthquakes is still in a consolidation phase. One study evaluated an eight-story building plus basement with SLB dissipaters, showing a decrease of up to 43.16% in distortions and 29.24% in shear forces with respect to a model without such devices [10]. Likewise, the hysteretic behavior of SLBs was investigated by means of modeling based on the unified mechanics theory, demonstrating their capacity to dissipate high levels of energy and prevent early structural failures [11]. In addition, different energy dissipaters implemented in Peruvian buildings have been analyzed, highlighting the importance of using formal seismic-resistant solutions, given the high rates of construction informality that increase seismic vulnerability [12].

In China, research on energy dissipaters has experienced significant advances in fragility and seismic resilience. A 2022 study, focusing on 3, 9, and 20 story buildings, showed 30% to 100% reductions in the probability of collapse by employing plastic energy demand as a criterion [13]. Likewise, the influence of the velocity power α on the damage distribution in 3, 6, 9, and 20 story frames was analyzed, determining that nonlinear dissipaters can increase vulnerability to high intensity earthquakes, although they are more effective in less severe motions [14]. In addition, a comprehensive review on improving seismic resilience in buildings highlighted the simplicity and low cost of passive systems versus active and semi-active approaches [15]. Another work employed machine learning to formulate fragility curves in reinforced concrete frames with infill, validating their accuracy in structures affected by the 2016 Taiwan earthquake [16]. A metallic dissipator that combines shear and bending was also developed, increasing ductility by 46 % with respect to conventional devices [17]. Additionally, the incorporation of TADAS dissipaters can withstand significant nonlinear deformations of up to 8% drift without exhibiting residual deformation or severe damage, increasing the lateral load capacity by 71 % to 90 % [18]. Finally, hybrid dissipaters demonstrated effectiveness by combining technologies, reducing drifts, displacements and stresses under a wide range of seismic intensities [19].

In Iran, several studies consolidated the use of energy dissipaters in steel and reinforced concrete frames. For example, curved TADAS dissipators in steel moment resisting frames showed a significant reduction in structural responses and failure prevention [20]. Another study pointed out that, in the rehabilitation of reinforced concrete frames with TADAS dampers, the increase in the number of plates and axial force in columns directly

influences the strength, stiffness and ductility of the system. Moreover, if the axial force exceeds a certain threshold, the energy dissipation capacity is significantly affected [21]. The use of X-dissipators in concrete portal frames was also analyzed, highlighting the importance of the dissipator stiffness [22]. Likewise, ADAS dissipators in steel walls increased the ductility and reduced the pinching phenomenon under cyclic loads [23]. In reinforced concrete moment resisting frames, ADAS showed better performance than TADAS with chevron bracing [24]. Additional studies concluded that the selection and arrangement of dissipaters in steel frames significantly affect the seismic response [25], highlighting the performance of friction dissipaters, which increased the energy absorption in Chevron portal frame connections by 32% [26].

In India, studies on seismic fragility of reinforced concrete buildings indicated that longer duration of seismic motion significantly increases the probability of collapse due to damage accumulation [27]. Other investigations concluded that soil-structure interaction is crucial for predicting seismic vulnerability [28]. In addition, rehabilitation techniques on damaged frames with steel bracing and hybrid metal dissipators achieved drifts of 3.5 % to 6 %, exceeding FEMA standards [29].

In France, a state-of-the-art study on passive systems on steel tie rods analyzed metallic, viscous and friction dissipaters, concluding that there is no single solution, as it depends on factors such as cost, duration and specific technical requirements [30].

In Spain and the United States, an auxiliary structure was designed in ABAQUS to test large displacements in SLB dissipaters, guaranteeing stability and stiffness [31].

In South Korea, energy dissipation in slender reinforced concrete elements was analyzed, concluding that it occurs mainly through the plastic behavior of reinforcing steel [32]. In Jordan, it was proposed to use calibrated probabilistic classifiers to predict brittleness curve parameters, obtaining more accurate results than traditional methods [33].

In Brazil, a methodology based on Concentrated Damage Mechanics was developed to evaluate seismic vulnerability of reinforced concrete frames, showing an accurate evaluation of collapse mechanisms, especially in irregular buildings [34].

In Ecuador, the performance of SLB dissipaters in decoupled walls showed reductions of more than 75 % in maximum floor shear and a remarkable improvement in energy dissipation [35].

In Italy, fragility curves in reinforced concrete frames with different regularities were investigated, showing that those based on the demand-rotation capacity ratio are more reliable [36]. Another study proposed a simplified methodology to assess vulnerability in historic buildings, validated with earthquakes that occurred in 1997 and 2016 [37]. It was further concluded that including undamaged buildings improves the accuracy of fragility curves when

analyzing post seismic data from the L'Aquila and Emilia earthquakes [38].

Overall, the analysis of the reviewed research evidences important advances in the implementation optimization of energy dissipation devices as an effective strategy to mitigate seismic risk and increase structural resilience globally. The results highlight that the proper selection of the type of dissipator, as well as an optimal configuration and strategic location within the structure, fundamental to guarantee efficient performance. Likewise, the generation and application of fragility curves are consolidated as essential tools to evaluate structural vulnerability to different levels of seismic intensity, providing accurate criteria for a performance-based design. This approach allows not only to reinforce structural safety, but also to optimize rehabilitation interventions in existing buildings, thus strengthening the effectiveness of mitigation strategies and improving the response capacity to future seismic events.

3. Materials and Methods

In this study, ADAS, TADAS and SLB type seismic dissipation devices were incorporated to analyze their influence on the structural behavior of buildings with different slenderness ratios. In order to quantify vulnerability, fragility curves were developed that relate seismic intensity to the probability of structural damage. For this purpose, an analysis based on the capacity curve and inelastic demand spectra was carried out, which allows determining the performance point and evaluating the influence of the seismic variability of the buildings. This approach provides a more complete view of the structural behavior under seismic stresses.

The analysis procedures used are presented, including the generation of structural models, the definition of seismic loading scenarios and the methodology adopted for the generation of fragility curves.

3.1. Seismic Parameters

Following the provisions of the Seismic Resistant Design Technical Standard E.030 [39], the analyzed buildings were analyzed for residential use and classified as category C buildings, with a use factor U=1.00. The location considered is the city of Lima, Peru, a region located in seismic zone Z4, corresponding to a seismic factor Z=0.45. The soil type was classified as "S1 - Rock or Very Rigid Soils" and, based on both this classification and the seismic zone, a soil factor S=1.00 was determined.

As for the basic reduction coefficient (Ro), different values were used depending on the structural direction. In the Y direction, a structural wall system with Ro=6.00 was used, while in the X direction a portal frame system with Ro=8.00 was adopted. It should be noted that the structural configuration of these buildings does not present irregularities, neither in plan nor in height.

3.2. Vertical Loads in Buildings

Regarding gravity actions, a detailed analysis of vertical loads was carried out considering the provisions specified in the Technical Load Standard E.020 [40]. This analysis included both dead loads, related to the self-weight of structural elements such as columns, beams, slabs and walls, as well as finishes and permanent components, for which a uniform value of 1.0 kN/m²was assumed. In addition, live loads corresponding to the residential use of the buildings were incorporated, considering a load of 2.0 kN/m²for interior environments such as corridors and stairways, in accordance with the aforementioned standards. In this way, it was ensured that the load scenarios adequately reflect the real conditions to which the buildings are exposed, providing a solid basis for evaluating their structural response.

3.3. Geometric Configuration and Slenderness Ratio in the Analyzed Structures

To evaluate the influence of slenderness on the effectiveness of the energy dissipaters in seismic events, three slenderness ratios, defined as the ratio between the total height of the building and the smallest dimension in plan, were analyzed. These ratios were 1, 2 and 3, corresponding to 6, 12 and 18 story buildings, respectively, keeping the floor plan dimensions constant in order to clearly isolate the effect of height on structural performance. The geometric characteristics adopted in each case are summarized in Table 1.

Table 1. Geometric parameters of the buildings for their respective modeling

Geometric characteristics	Building 1	Building 2	Building 3
Mezzanine height	3.00 m	3.00 m	3.00 m
Overall height	18.00 m	36.00 m	54.00 m
Dimension X	18.00 m	18.00 m	18.00 m
Dimension Y	25.00 m	25.00 m	25.00 m
Number of levels	6	12	18
Slenderness	1	2	3

The selection of these values is due to the fact that slenderness directly influences lateral stiffness and, consequently, the dynamic response of the building to seismic events. Thus, structures with greater slenderness tend to present more significant lateral displacements due to their inherent flexibility, which increases their seismic demand and requires the effective incorporation of energy dissipation systems to mitigate possible damage. In contrast, buildings with lower slenderness have higher lateral stiffness, which usually results in smaller displacements, but could limit the efficiency of dissipaters if they are not specifically designed for low-deformation conditions [9]. Schematically, Figure 1 presents the structural configurations studied for each slenderness ratio, generated using ETABS structural modeling software [41], facilitating a clear visualization of the approach taken in the analysis.



Figure 1. Structural configuration of the buildings analyzed with different slenderness ratios generated using ETABS software

Concrete		Reinforci	ng Steel	Structural Steel		
Material	Value	Material	Value	Material	Value	
$\gamma (kN/m^3)$	24.00	$\gamma (kN/m^3)$	78.50	$\gamma (kN/m^3)$	78.50	
f'c (kN/m²)	21.00 28.00 35.00	f'c (kN/m²)	420.00	f'c (kN/m²)	253.00	
E (kN/m²)	4700√f°c	E (kN/m²)	200000.00	E (kN/m²)	200000.00	
μ	0.15	-	-	μ	0.30	

Table 2. Assumed properties of materials for the modeling of structures

3.4. Mechanical Properties of Materials

The mechanical properties of the materials used in the structural components of the buildings analyzed are detailed in Table 2, which presents the specific characteristics of the concrete, reinforcing steel and structural steel used in the buildings. These properties were determined according to the technical specifications established in the Peruvian Technical Standards E.020 [40] and E.060 [42], guaranteeing reliable results for structural analysis. In this table, f'c corresponds to the compressive strength of the concrete, fy to the yield strength of the steel, γ to the specific weight, E to the modulus of elasticity, and μ to Poisson's modulus.

3.5. Configuration and Dimension of Structural Elements

The structural configuration proposed in this study, representative of Peruvian buildings, is characterized by the arrangement of structural walls predominantly in a single direction, due to architectural restrictions imposed by the boundaries. To guarantee efficient seismic performance, fundamental principles of Seismic Resistant Structural Design were applied, such as symmetry in the distribution of masses and stiffness, structural continuity in plan and elevation, and adequate resistance to lateral loads in both main directions. In addition, ductility, lateral deformation control and structural redundancy were prioritized to improve safety and performance in severe seismic events [43], [44], [45].

Regarding the geometric properties of the structural elements, columns with dimensions of 50 cm x 90 cm, reinforced concrete walls with thicknesses of 30 cm in the "Y" direction and 40 cm in the "X" direction, 30 cm x 50

cm beams in all directions, and 15 cm thick solid slabs were used. This configuration was kept uniform in all the structures analyzed, varying only the number of levels to evaluate the impact of slenderness on seismic behavior. The distribution of these elements, as well as the labels used to differentiate the reinforcement schemes in the beams, can be seen in Figure 2.

Regarding the properties of the materials used, a concrete with a compressive strength of f'c = 21 kN/m^2 was used for the beams and solid slabs in all structural configurations. For the building with slenderness 1, the columns and walls were assigned a concrete with a compressive strength f'c = 21 kN/m^2 . In the building with slenderness 2, a concrete with f'c = 28 kN/m^2 was used from the first to the sixth floor, while from the seventh to the twelfth floor a concrete of f'c = 21 kN/m^2 was used. Finally, in the building with slenderness 3, three levels of resistance were established: f'c = 35 kN/m^2 in the first six levels, f'c = 28 kN/m^2 between the seventh and twelfth floors, and f'c = 21 kN/m^2 from the thirteenth to the eighteenth level. This distribution of resistances is presented in Figure 3.

Table 3 presents the details of column reinforcement, showing the distribution of longitudinal and transverse reinforcement used in all structural configurations. Table 4 describes the reinforcement of the beams, differentiating the upper and lower reinforcement according to the defined schemes. These configurations follow the labels established in Figure 2, facilitating the correct location and understanding of the structural reinforcement in the analysis.

Overall, the standardization of both the distribution of reinforcement and the arrangement of structural elements allows for an objective and consistent evaluation of seismic behavior at different slenderness ratios.

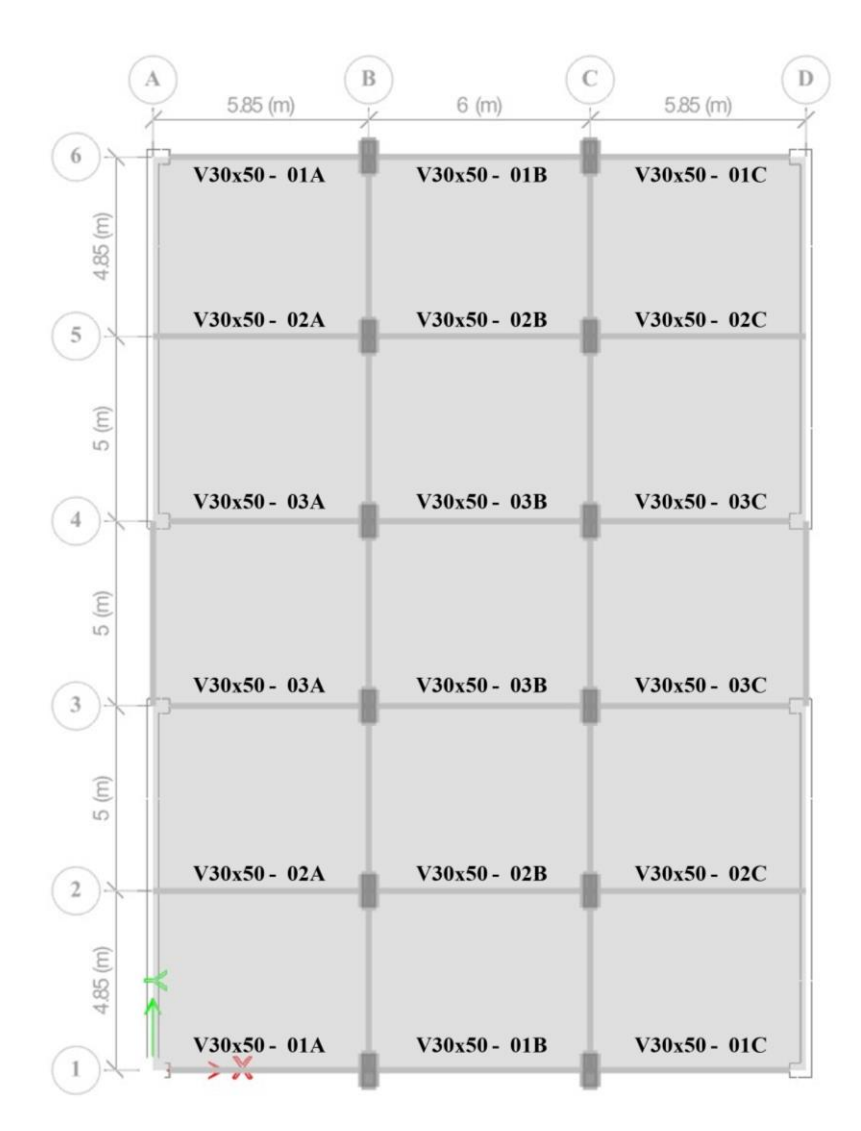


Figure 2. Distribution of structural elements and labeling of beams in the analyzed models

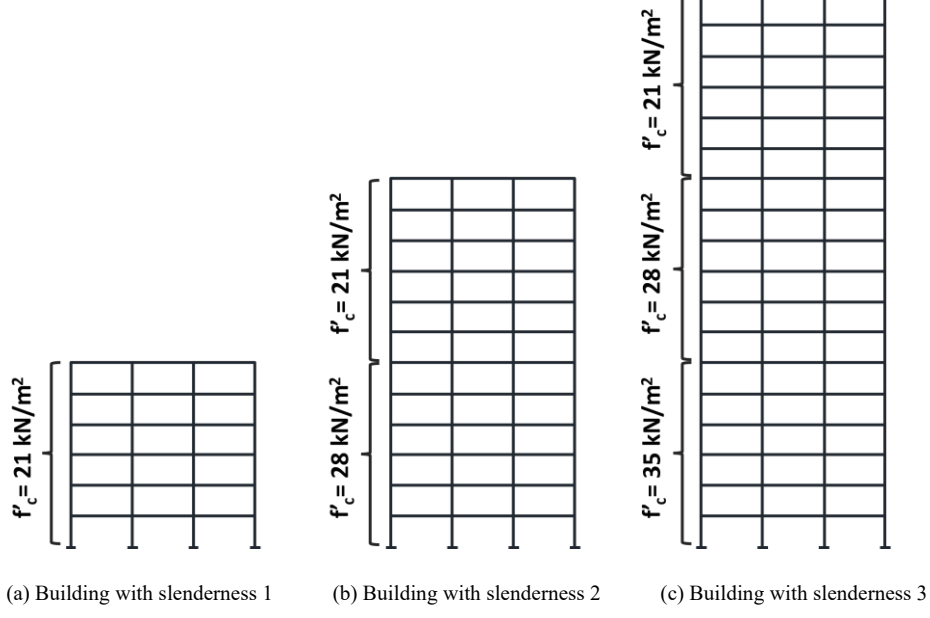


Figure 3. Distribution of concrete strength in columns and walls according to the slenderness of the building

C50x90
35kN/m²

C50x90
28kN/m²

21kN/m²

.50

.50

.90

.16Ø 3/4"

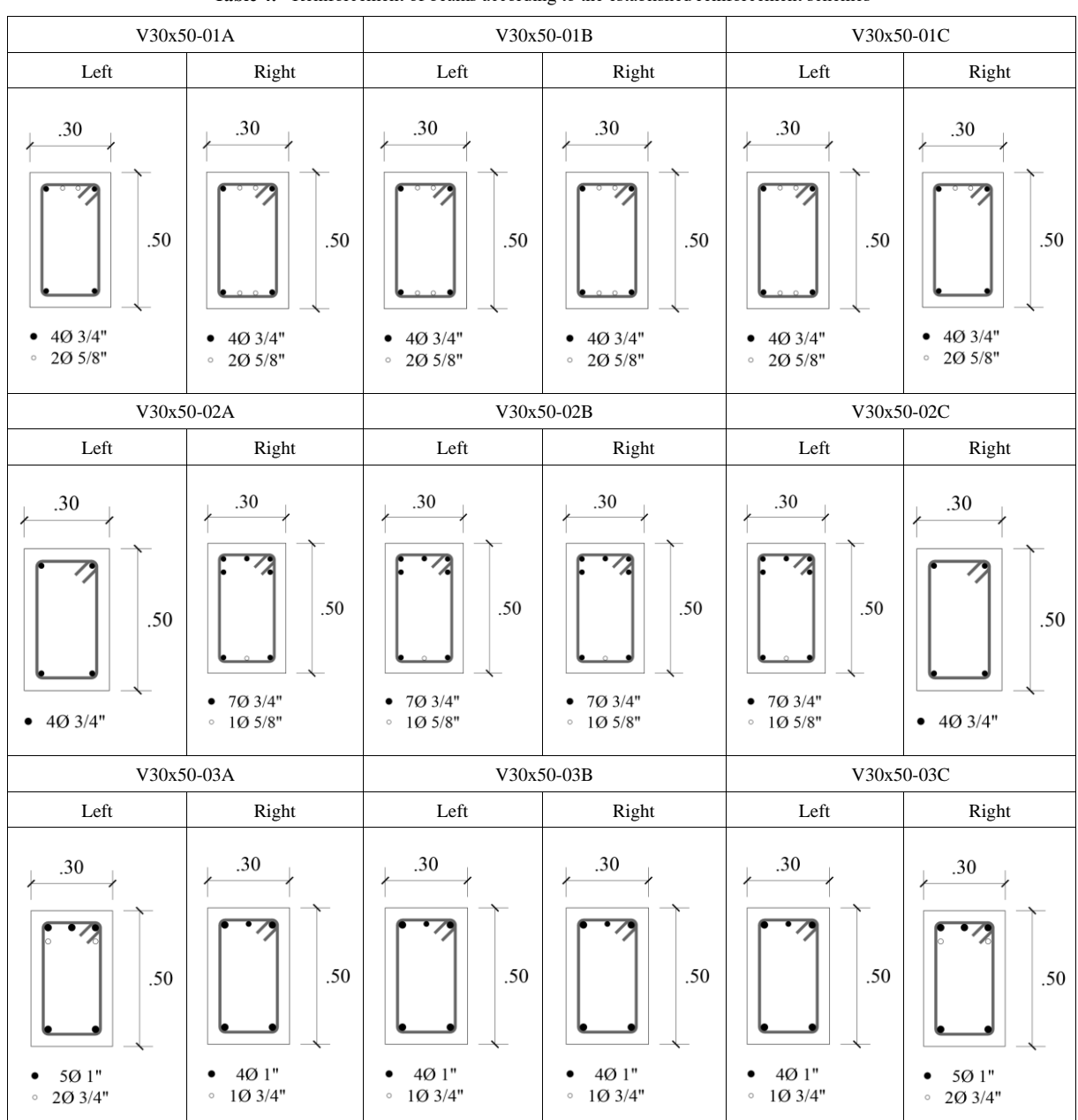
.16Ø 3/4"

.16Ø 3/4"

.16Ø 3/4"

Table 3. Column reinforcement in the analyzed structural configurations

Table 4. Reinforcement of beams according to the established reinforcement schemes



3.6. Bracing Configuration

A common construction method for the incorporation of seismic dissipation devices in structures is the use of concentric bracing in an inverted V or Chevron configuration, built in steel and directly connected to the dissipation devices, as illustrated in Figure 4. In this configuration, the top joint acts as a panel zone, avoiding the transmission of axial loads and concentrating the nonlinearity in the connections, which improves the seismic response by reducing deformations and efficiently distributing the seismic forces [46], [47].

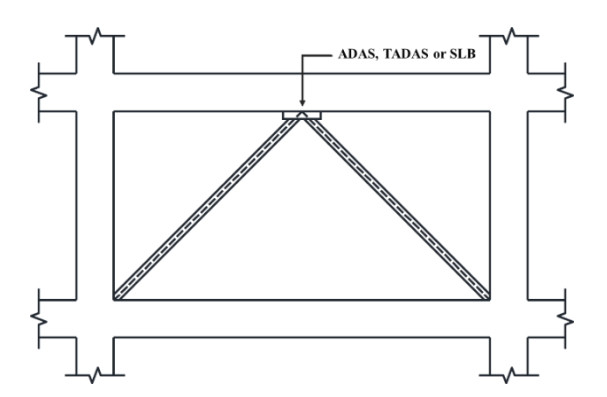


Figure 4. Configuration of concentric chevron bracing connected to the dissipaters

To optimize the control of displacements and forces, the bracing was strategically placed in axes 1 and 6, between axes AB and CD. These elements have dimensions of 20 cm x 20 cm and a thickness of 3/8" and serve as support for the installation of the ADAS, TADAS and SLB devices, as shown in Figure 2.

3.7. Properties of Seismic Dissipation Devices

The seismic dissipation devices used in buildings are of the hysteretic type. These are illustrated in more detail in Figure 5, where (a) corresponds to ADAS [49], (b) to TADAS [49] and (c) to SLB [50].

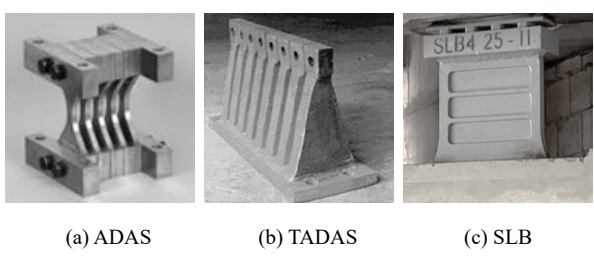


Figure 5. Hysteretic dissipators

These devices are designed to transform seismic energy into thermal energy through the controlled plasticization of metallic elements, reducing the demands on the main structural elements and improving the overall performance of buildings in seismic events, thus ensuring greater structural safety [48].

ADAS employs X - shaped plates or cruciform elements that deform plastically through repeated bending, concentrating energy dissipation in the most susceptible areas [49]. TADAS, on the other hand, uses triangular plates whose thinner sections concentrate stresses and facilitate energy dissipation in each seismic cycle [49]. For its part, the SLB is based on the eccentric bracing system, presenting a wide flange section that is machined from a flat section. This process avoids the need for welds, allowing the forming of thin zones for energy dissipation [50].

The mechanical properties of ADAS and TADAS dissipators were calculated using the equations presented in [49], based on a bilinear hysteresis diagram. Table 5 summarizes these equations, in which n represents the number of plates, fy the yield strength of the steel, b the base of the dissipator, h its height, t the plate thickness and E the modulus of elasticity of the material. The results obtained from these expressions are presented in Tables 6 and 7, which show, respectively, the development of the theoretical equations and the numerical values calculated for each type of dissipator.

Table 5. Derived equations for the calculation of the mechanical properties of ADAS and TADAS dissipaters based on a bilinear hysteresis diagram

Parameter	ADAS	TADAS
Creep strength	$F_y = \frac{nf_y b_1 t^2}{3h}$	$F_{y} = \frac{nf_{y}b_{1}t^{2}}{6h}$
Creep displacement	$\Delta_y = \frac{f_y h^2}{2Et}$	$\Delta_{y} = \frac{f_{y}h^{2}}{Et}$
Elastic stiffness	$K_{DDE} = \frac{2nEb_1t^3}{3h^3}$	$K_{DDE} = \frac{nEb_1t^3}{6h^3}$
Ultimate strength	$F_u = n \frac{f_y b_1 t^2}{2h}$	$F_u = n \frac{f_y b_1 t^2}{4h}$

In the case of SLB dissipaters, their mechanical properties were not determined experimentally. Instead, the parameters provided by the manufacturer's official datasheet, which describes their strength and performance characteristics under cyclic loading, were used. This extracted from the information, SLB documentation [50], is summarized in Table 8.

3.8. Design of Energy Dissipation Systems

The implementation of seismic dissipation devices aims to provide the necessary stiffness to the structure to maintain the maximum interstory distortion below the allowable limit of 0.007, as established in the E.030 Seismic Resistant Design Standard [39]. For this purpose, the installation of chevron type steel frames with such devices is proposed, which helps to reduce the interstory distortions and guarantees an adequate structural performance against seismic events.

The devices selected to meet the performance requirements are presented in Table 9.

 Table 6.
 Parameters derived from the proposed equations for the ADAS dissipaters

Tipo	n	h (cm)	b (cm)	Fy (kN)	Δy (mm)	KDDE (KN/m)	Fu (kN)	Kp (kN/m)	Δu (mm)	KEDDE (kN/m)
ADAS_1	1	30.00	15.00	27.20	2.13	12745.49	40.81	637.27	21.34	1911.82
ADAS_2	2	30.00	15.00	54.41	2.13	25490.99	81.61	1274.55	21.34	3823.65
ADAS_3	3	30.00	15.00	81.61	2.13	38236.48	122.42	1911.82	21.34	5735.47
ADAS_4	4	30.00	15.00	108.82	2.13	50981.98	163.23	2549.10	21.34	7647.30
ADAS_5	5	30.00	15.00	136.02	2.13	63727.47	204.03	3186.37	21.34	9559.12
ADAS_6	6	30.00	15.00	163.23	2.13	76472.97	244.84	3823.65	21.34	11470.94
ADAS_7	7	30.00	15.00	190.43	2.13	89218.46	285.64	4460.92	21.34	13382.77
ADAS_8	8	30.00	15.00	217.63	2.13	101963.95	326.45	5098.20	21.34	15294.59
ADAS_9	9	30.00	15.00	244.84	2.13	114709.45	367.26	5735.47	21.34	17206.42
ADAS_10	10	30.00	15.00	272.04	2.13	127454.94	408.06	6372.75	21.34	19118.24

 Table 7. Parameters derived from the proposed equations for the TADAS dissipaters

Tipo	n	h (cm)	b (cm)	Fy (kN)	Δy (mm)	KDDE (KN/m)	Fu (kN)	Kp (kN/m)	Δu (mm)	KEDDE (kN/m)
ADAS_1	1	30.00	15.00	13.60	4.27	3186.37	20.40	159.32	42.69	477.96
ADAS_2	1	30.00	15.00	13.60	4.27	3186.37	20.40	159.32	42.69	477.96
ADAS_3	3	30.00	15.00	40.81	4.27	9559.12	61.21	477.96	42.69	1433.87
ADAS_4	4	30.00	15.00	54.41	4.27	12745.49	81.61	637.27	42.69	1911.82
ADAS_5	5	30.00	15.00	68.01	4.27	15931.87	102.02	796.59	42.69	2389.78
ADAS_6	6	30.00	15.00	81.61	4.27	19118.24	122.42	955.91	42.69	2867.74
ADAS_7	7	30.00	15.00	95.21	4.27	22304.61	142.82	1115.23	42.69	3345.69
ADAS_8	8	30.00	15.00	108.82	4.27	25490.99	163.23	1274.55	42.69	3823.65
ADAS_9	9	30.00	15.00	122.42	4.27	28677.36	183.63	1433.87	42.69	4301.60
ADAS_10	10	30.00	15.00	136.02	4.27	31863.74	204.03	1593.19	42.69	4779.56

Table 8. Design parameters of the SLB dissipater according to the data sheet provided by the manufacturer

ID	Device	K1 (kN/cm)	K2 (kN/cm)	r=K2/K1	Fy (kN)	Fmax (kN)	K(U3) (kN/cm)	Kr(U1) (kN/cm)
417	SLB4 10_5	2026.65	21.622	0.010669	151.792	250.004	96	480
418	SLB4 10_6	2163.531	22.9	0.010585	160.536	265.784	142	710
419	SLB4 15_5	2472.601	24.855	0.010052	177.92	293.725	142	1420
420	SLB4 15_6	2761.73	26.96	0.009762	195.094	320.623	143	1430
421	SLB4 15_7	3021.879	28.761	0.009518	210.756	345.093	143	1430
422	SLB4 20_6	3360.997	33.085	0.009844	230.931	381.615	158	2370
423	SLB4 20_7	3700.15	35.278	0.009534	248.979	410.695	158	2370
424	SLB4 25_6	4260.805	42.532	0.009982	278.739	468.957	305	4575
425	SLB4 25_7	4767.675	46.508	0.009755	304.308	512.315	306	4590
426	SLB4 25_8	5238.65	50.431	0.009627	327.733	552.765	307	4605

Table 9. Specifications of the dissipation devices used in studio configurations

Dissipater	Dissipater Slenderness 1		Slenderness 3
ADAS	ADAS_9	ADAS_9	ADAS_9
TADAS	TADAS_9	TADAS_9	TADAS_9
SLB	SLB4 25_7	SLB4 25_8	SLB4 25_8

3.9. Seismic Records

Seven seismic records obtained from [51] were used. the details of which are presented in Table 10. It assigns a name to each record and includes the date, maximum ground accelerations in the north-south (PGA-NS) and east-west (PGA-EW) directions, as well as the magnitude and duration of the earthquake. For this study, representative earthquakes of our country and some recent records were selected in order to cover different scenarios and local conditions.

Table 10. Main characteristics of the seismic records used in the study

Location	Date	PGA NS (g)	PGA EW(g)	Magnitude
Arequipa	17-07-2017	0.04	0.04	6.8 Mw
Atico	23-06-2001	0.29	0.29	6.9 mb
Huaraz	31-05-1970	0.11	0.10	6.6 mb
Lima	17-10-1966	0.18	0.27	8.1 Mw
Lima	03-10-1974	0.19	0.18	6.6 mb
Pisco	15-08-2007	0.30	0.37	7.0 ML
Tacna	21-11-2017	0.10	0.10	6.3 ML

Figures 6 and 7 show the corrected records of the 2007 Pisco earthquake in the East-West (EW) and North-South directions, respectively. These records (NS)

processed and subjected to baseline correction using specialized seismology software [52], [53].

Figure 8 shows the response spectrum of the natural records with a damping of 5%. It can be seen that, in short periods, most of them generate high accelerations, which gradually attenuate and decrease significantly as the periods increase. The earthquake with the highest spectral acceleration corresponds to Pisco (a ≈ 1.34 g), followed by Lima (a ≈ 0.97 g).

For the scaling of the accelerograms, eight PGA levels with 0.1 g increments were considered, scaling each record to the corresponding intensity level.

3.10. Methodology for Obtaining Fragility Curves

To obtain the fragility curves, a procedure based on the FRACAS method [54] was followed, which allows their generation from spectra derived from seismic records, incorporating the variability of the seismic movement and the structural characteristics of the buildings.

The nonlinear analysis, required in this process, was carried out according to the recommendations of Appendix A of ACI 318-19 [55] and the guidelines for component models described in NIST GCR 10-917-5 [56]. Plastic patellae in the beams (concentrated plasticity) and a fiber model in the columns (distributed plasticity) were assigned in accordance with ASCE/SEI 41-17 [57].

To ensure the representativeness of the obtained fragility curves, a set of seismic records scaled to different intensity levels was used, allowing to evaluate the probability of damage as a function of the imposed seismic demand. The selection and scaling of these records were carried out following criteria that ensure an adequate coverage of the range of seismic intensities expected at the study site, minimizing biases in the estimation of structural fragility.

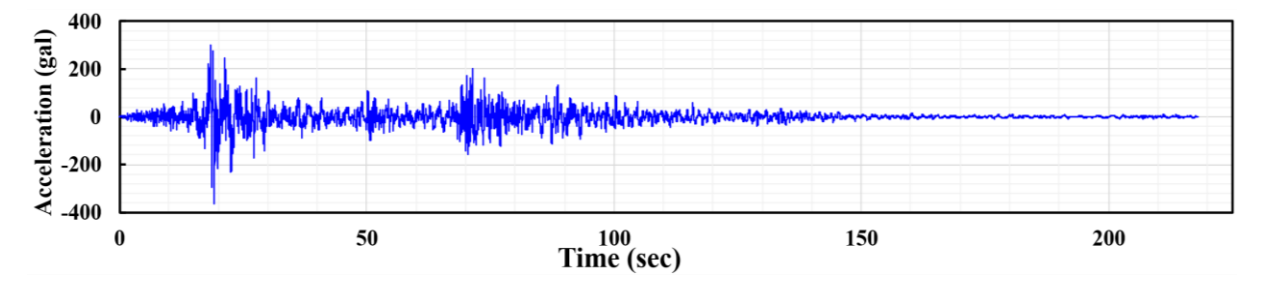


Figure 6. Record of the 2007 Pisco earthquake in the North-South (NS) direction after the baseline correction process

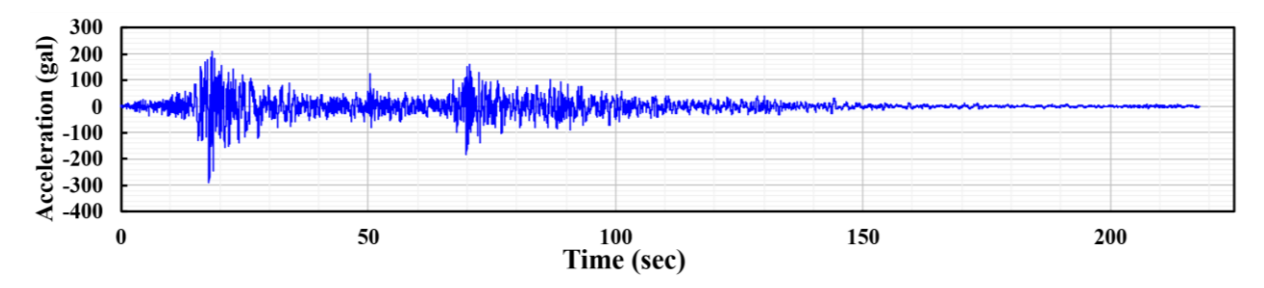


Figure 7. Record of the 2007 Pisco earthquake in the East-West (EW) direction after the baseline correction process

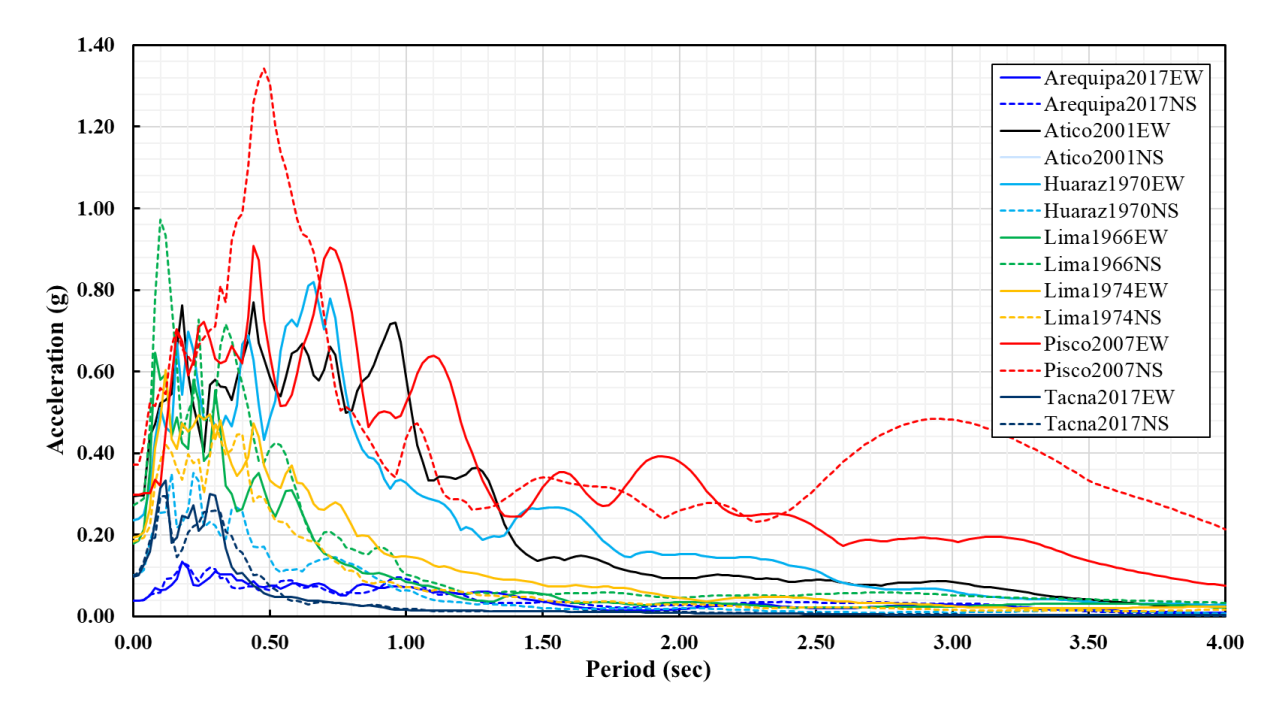


Figure 8. Response spectra with 5% damping for natural seismic records

Figure 9 presents the process diagram corresponding to this methodology, visually structuring each of the steps developed.

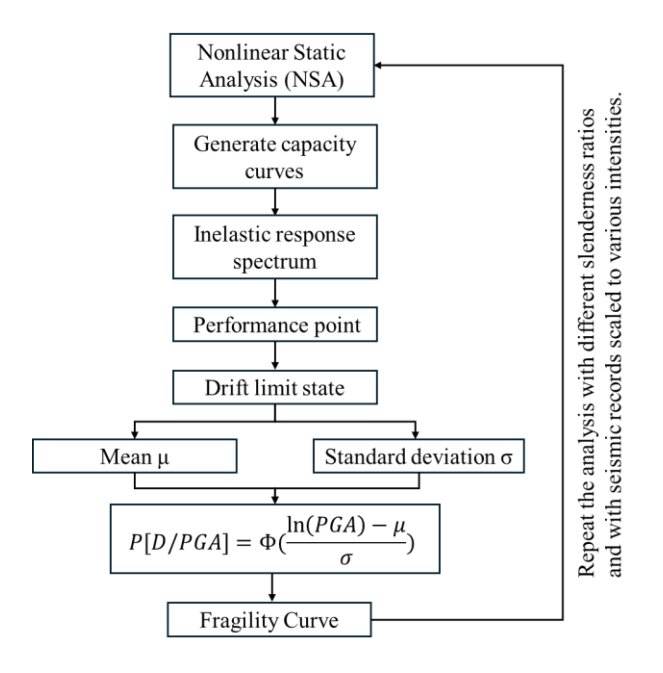


Figure 9. Process diagram for obtaining fragility curves based on the FRACAS methodology

3.11. Performance Evaluation

To evaluate the performance in this case study, three damage states were considered according to the FEMA 356 criteria [58], which establish interstory drift limits as a function of structural type. In this work, these values

were used to define the damage states in the superstructure. Table 11 presents the drift limits adopted for the analyzed structural typology.

Table 11. Maximum floor drift ratio limit for each performance category

Limit state	Drift coefficient
Immediate Occupancy	0.005
Life Safety	0.015
Collapse Prevention	0.020

With these values, the peak ground accelerations (PGA) associated with each limit state were determined and their respective means and standard deviations were calculated. These results will allow us to evaluate the structural fragility of the superstructure and its response to different levels of seismic demand.

4. Results

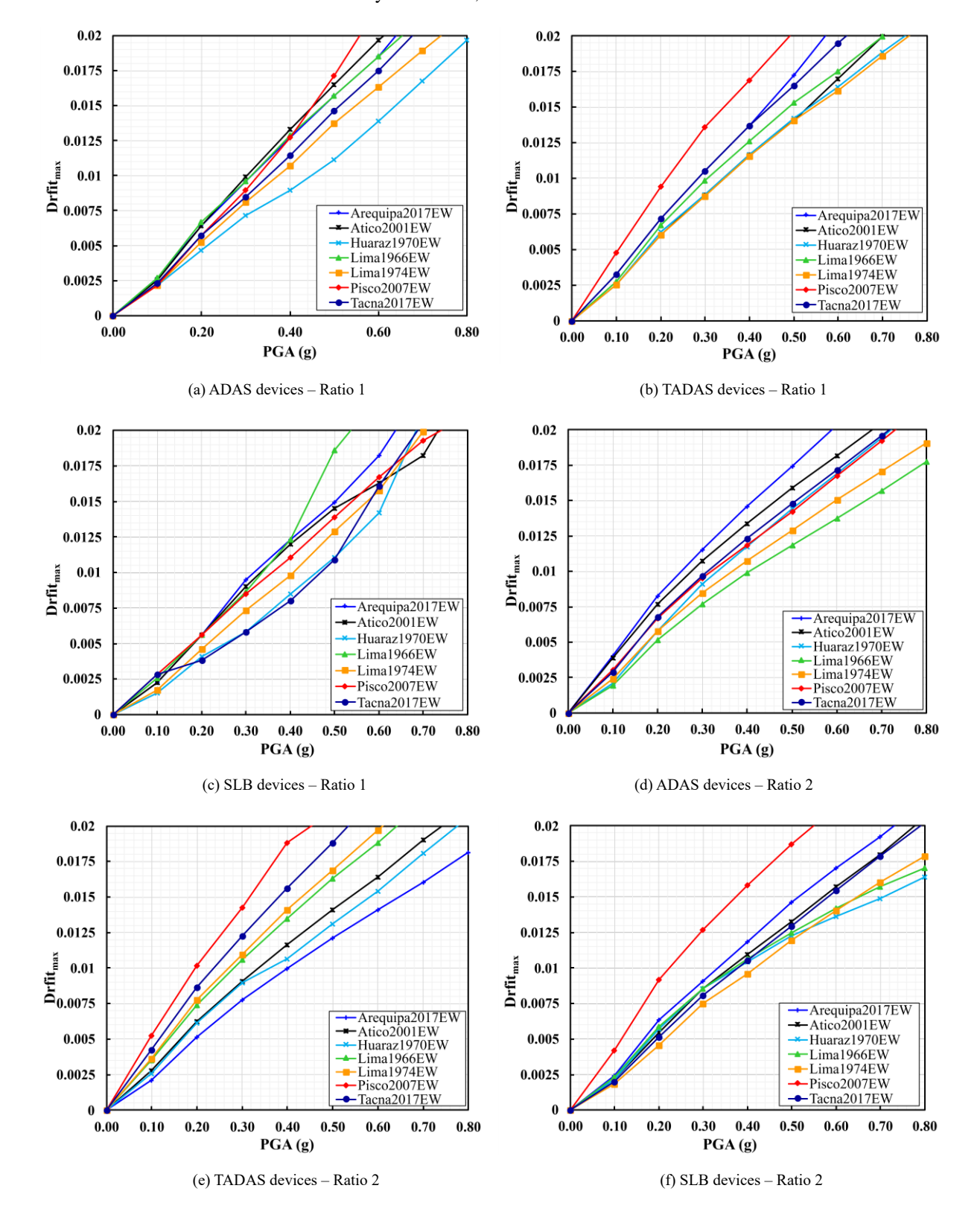
In this study, fragility curves were analyzed for buildings with three levels of slenderness 1, 2 and 3, considering the influence of ADAS, TADAS and SLB type seismic dissipaters. The probability of the structure reaching or exceeding different seismic performance states, defined as Immediate Occupancy (IO), Life Safety (LS) and Collapse Prevention (CP), was evaluated as a function of the PGA.

4.1. Relationship between PGA and Max Drift

Following the methodology described in section 3.10.,

structural performance points were determined and PGA (g) vs. drift plots were generated to evaluate the structural behavior. Figure 10 shows this relationship for the analyzed models.

The results obtained after evaluating the relationship between PGA and maximum drift for the analyzed models, presented here, reveal notable differences in the structural response according to the type of dissipator used and the slenderness. In the following, the values recorded for PGA of 0.2g and 0.5g for the Pisco2007EW seismic record are specifically discussed, highlighting the observed.



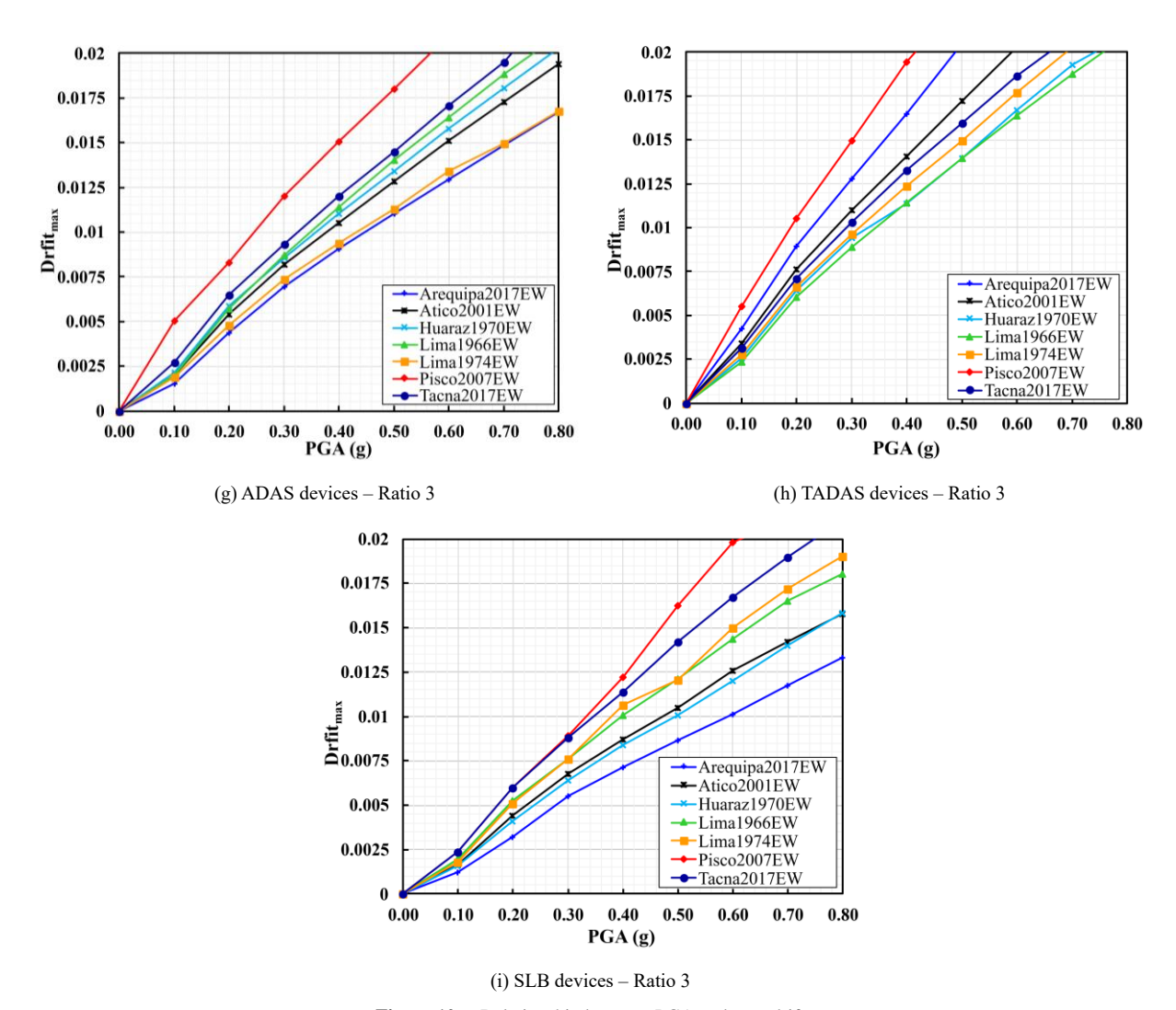


Figure 10. Relationship between PGA and max drift

In buildings with a slenderness ratio equal to 1, maximum drifts of 0.0057, 0.0094 and 0.0056 were obtained for Figures 10a, 10b and 10c, respectively, at a PGA of 0.2g. As the PGA increased to 0.5g, the drifts increased to 0.0171, 0.0203 and 0.0139, respectively. These percentage increases are equivalent to 200.00%, 115.96% and 148.21%.

For buildings with a slenderness ratio equal to 2, the drifts at a PGA of 0.2g were 0.0067, 0.0102 and 0.0092 in Figures 10d, 10e and 10f, respectively. With the increase of the PGA to 0.5g, these drifts reached values of 0.0142, 0.0210 and 0.0187, showing percentage variations of 111.94%, 105.88% and 103.26%. In this slenderness, the relative increases between the different dissipators are comparable.

Finally, for buildings with a slenderness ratio equal to 3, at a PGA of 0.2g, the maximum drifts were 0.0083, 0.0105 and 0.0060 for Figures 10g, 10h and 10i, respectively. By increasing the PGA to 0.5g, these drifts increased to 0.0180, 0.0230 and 0.0163, representing percentage increases of 116.87%, 119.05% and 171.67%, respectively.

The results obtained allow determining that the

structural performance is significantly influenced by the type of dissipater used and the slenderness of the building. Consistently, the SLB type dissipater presented lower absolute drift values in all the configurations analyzed, highlighting its effectiveness especially in structures with greater slenderness.

4.2. Validation of Static Nonlinear Analysis

Although static nonlinear analysis is an effective tool, it presents certain limitations as established in ASCE/SEI 41-17 [57], particularly in structures with complex configurations or significant nonlinear behaviors. To overcome these restrictions and ensure the reliability of the results obtained, the study was complemented with a dynamic nonlinear analysis. This procedure made it possible to verify and validate the initial results of the static nonlinear analysis. Figure 11 presents the comparison between the basal shear obtained from the static analysis and dynamic analysis, specifically Pisco2007EW seismic record, from which it can be seen that the basal shear obtained from the static analysis is higher than that of the dynamic analysis.

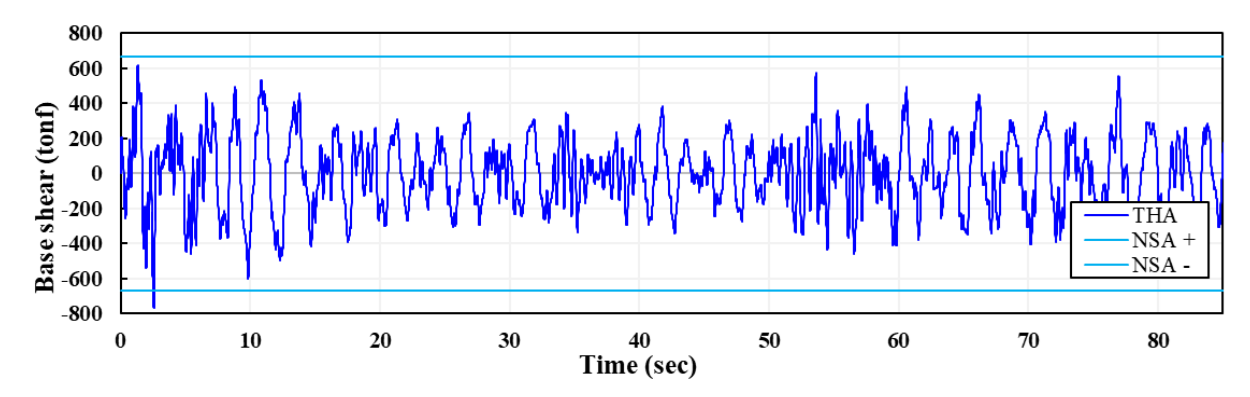


Figure 11. Comparison of basal shear obtained by static nonlinear analysis and dynamic nonlinear analysis for the Pisco2007EW seismic record

4.3. Fragility Curves

From the relationship between PGA and Maximum Drift, the μ (mean) and σ (standard deviation) of the natural logarithm of PGA were determined for the three damage states established in Item 3.11. The values obtained are tabulated in Tables 12, 13 and 14.

Table 12. Log-normal distribution parameters for ADAS devices

ADAS	Immediate Occupancy				Collapse Prevention	
Ratio	μ	σ	μ	σ	μ	σ
1	0.178	0.110	0.508	0.132	0.670	0.125
2	0.159	0.167	0.529	0.155	0.741	0.143
3	0.177	0.228	0.576	0.188	0.824	0.175

Table 13. Log-normal distribution parameters for TADAS devices

TADAS	Immediate Occupancy				Collapse Prevention	
Ratio	μ	σ	μ	σ	μ	σ
1	0.151	0.156	0.475	0.153	0.656	0.152
2	0.144	0.235	0.478	0.243	0.664	0.226
3	0.151	0.156	0.475	0.153	0.657	0.194

Table 14. Log-normal distribution parameters for SLB devices

SLB	Immediate Occupancy		Life Safety		Collapse Prevention	
Ratio	μ	σ	μ	σ	μ	σ
1	0.2067	0.1751	0.5396	0.1035	0.6752	0.1038
2	0.1758	0.1752	0.5781	0.1902	0.8208	0.1942
3	0.1509	0.1558	0.4750	0.1530	0.6571	0.1936

From the results obtained, fragility curves were generated for all the models analyzed, allowing a detailed evaluation of their structural behavior under different levels of seismic intensity. These curves provide key information on the probability of damage as a function of the intensity of seismic movement, facilitating the comparison of the performance of buildings with different slenderness ratios and energy dissipation systems.

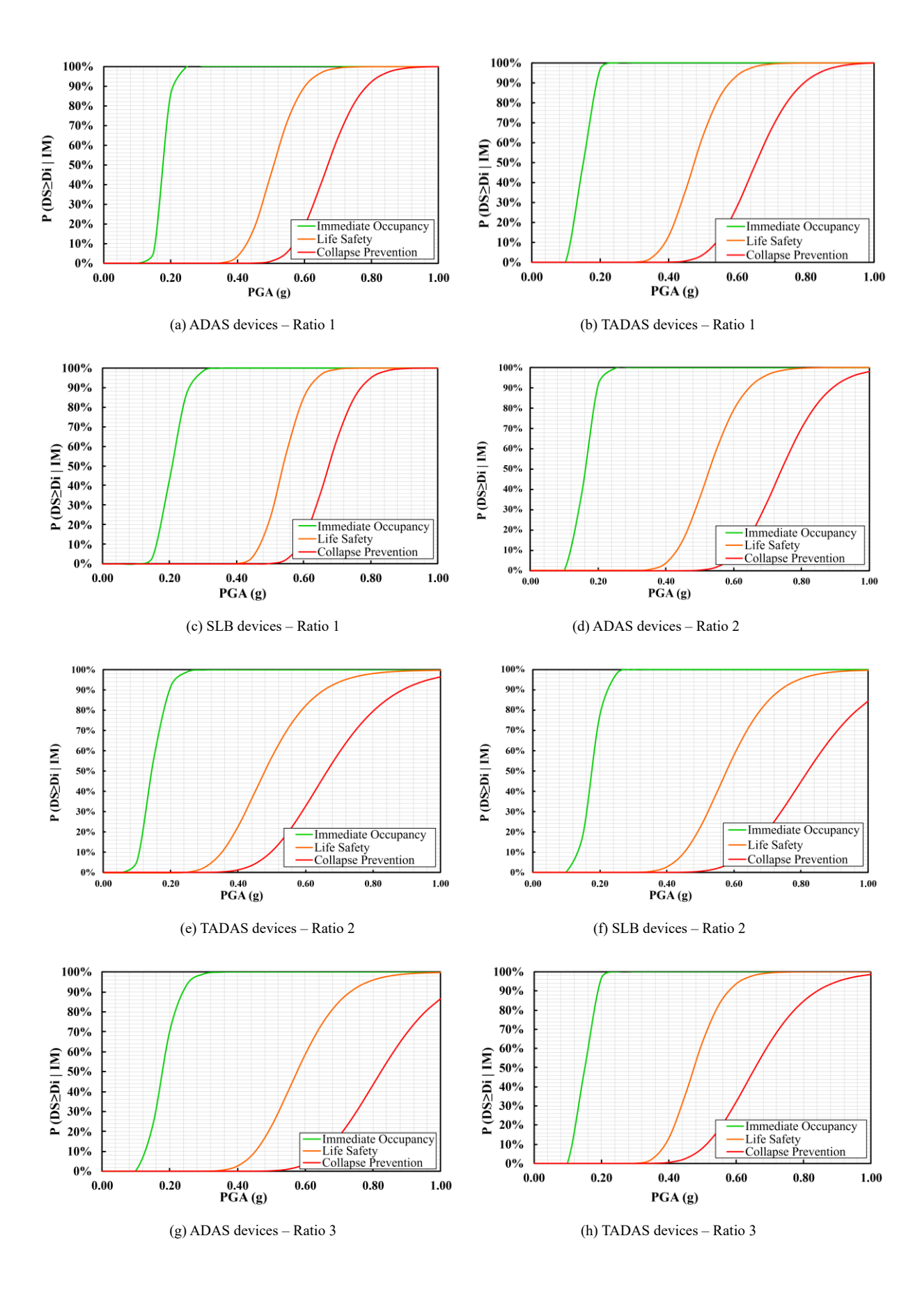
Figure 12 presents the fragility curves obtained for each structural configuration studied.

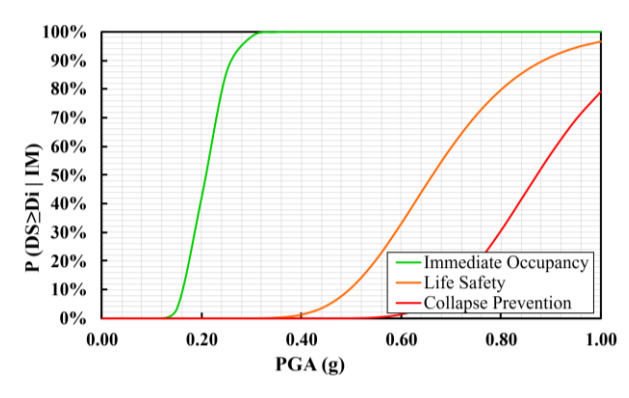
The results obtained after evaluating the fragility curves at three specific levels of PGA 0.25g, 0.50g and 0.75g show notable differences depending on the type of dissipater used and the slenderness of the structure. In buildings with a slenderness ratio equal to 1, the probabilities of exceeding the Immediate Occupancy level were practically 100% for all dissipative systems in Figures 12a, 12b and 12c at a PGA of 0.25g. By increasing the PGA to 0.50g, the exceedance probabilities of the Life Safety state were 45.18%, 63.12%, and 23.07%, respectively. For the Collapse Prevention level, the probabilities at PGA of 0.75g were significant: 81.63% in Figure 12a, 81.07% in Figure 12b and 84.44% in Figure

For buildings with a slenderness ratio equal to 2, at a PGA of 0.25g, the probabilities of Immediate Occupancy were again close to 100% in all configurations according to Figures 12d, 12e and 12f. Raising the PGA to 0.50g, the probabilities in the Life Safety state were 36.02% in Figure 12d, 57.22% in Figure 12e and 22.25% in Figure 12f. At the Collapse Prevention level, at PGA of 0.75g, the probabilities were 53.25% in Figure 12d, 70.54% in Figure 12e and 32.12% in Figure 12f.

Finally, for buildings with a slenderness ratio equal to 3, at a PGA of 0.25g the probabilities of Immediate Occupancy were 93.60% in Figure 12g, 99.94% in Figure 12h and 86.10% in Figure 12i. As the PGA increased to 0.50g, the Life Safety probabilities were 22.55%, 63.12% and 10.70%, respectively. At the Collapse Prevention level, for a PGA of 0.75g, the probabilities reached values of 29.47% in Figure 12g, 75.26% in Figure 12h and 18.80% in Figure 12i.

The structural performance depends significantly on the type of dissipater used and the slenderness of the building. The SLB type dissipater presented, in general, lowers probabilities of exceeding the critical performance levels, highlighting especially its effectiveness in structures with greater slenderness. This analysis highlights importance of properly selecting the dissipative system according to the specific structural characteristics in order to optimize seismic performance.





(i) SLB devices - Ratio 3

Figure 12. Fragility curves

5. Discussions

The results obtained in this research on the incidence of slenderness and the comparison of ADAS, TADAS and SLB dissipaters show agreement with previous studies focused on the influence of geometric variations on the performance of hysteretic devices. In particular, previous research on dissipaters in reinforced concrete structures [13] identifies that taller buildings require devices with lower stiffness and lower creep forces, a trend confirmed by our results, where the increase in slenderness implies an increase in the allowable displacements, requiring adjustments in the mechanical properties of the dissipaters.

Likewise, the superior effectiveness of the SLB dissipator observed especially in buildings slenderness 2 and 3 is related to that reported by previous studies [14], where the relevance of structural flexibility to optimize energy dissipation through adequate structural deformations is emphasized. Although this previous study does not directly address slenderness, its conclusions on the positive influence of structural flexibility in SLB-type devices agree with the results obtained in our study, which highlight the better response of the SLB dissipator as slenderness increases.

On the other hand, previous work on parametric analysis of seismic fragility [5] highlights the importance of factors such as stiffness and structural properties to estimate the probability of seismic damage by means of curves. Our research complements perspective by demonstrating how the variation in slenderness affects these probabilities. Likewise, it was observed that more flexible structures, with greater slenderness, present fragility curves shifted towards higher damage probabilities, confirming that geometry significantly influences seismic performance.

In the same vein, the favorable behavior of the SLB dissipater is supported by other studies [8], which highlight its effectiveness in reducing displacements and internal forces in mid-rise buildings. While those studies did not explicitly analyze variations in slenderness, their findings regarding the efficiency of SLB devices are consistent with our observations, reaffirming the advantages of SLB dissipaters over ADAS and TADAS in slender structural configurations.

From a practical standpoint, the findings of this research demonstrate that SLB-type dissipaters provide an effective and feasible solution for reinforced concrete buildings located in seismic zones, particularly those with slender or flexible structural systems. Their ease of implementation and proven efficiency in reducing lateral demands support their consideration in structural design guidelines and technical specifications, even in contexts where current codes do not explicitly regulate their use. In this context, incorporating parameters such as slenderness could contribute to the development of more efficient design strategies for buildings with similar structural characteristics.

6. Conclusions

The results confirm that the incorporation of ADAS, TADAS and SLB hysteretic dissipaters significantly improves the structural behavior in the face of increased PGA. Even in buildings of greater slenderness, where the risk of damage increases, the dissipaters delay the appearance of more critical performance states. However, notable differences were observed in the effectiveness of each dissipater depending on the geometric configuration of the structure.

The analysis performed on the three configurations studied showed that, as structural flexibility increases, so does the probability of reaching moderate or severe damage states. In structures with lower slenderness, the dissipators maintained low probabilities of critical damage even at high PGA levels. However, in structures with greater slenderness, vulnerability was more evident at PGA of 0.50g and above.

While all dissipaters contributed to reducing inelastic demand, the SLB dissipater performed more uniformly and effectively across all slenderness ranges, significantly delaying the onset of severe damage states. The ADAS and TADAS dissipaters performed favorably at lower slendernesses, but more rapidly increased the probability of reaching critical states in structures with high

slenderness.

These findings highlight the critical need to carefully match the mechanical properties of dissipaters, such as stiffness and yield strength, to the specific slenderness of the structure. For low-rise structures, devices that are too stiff may not activate effectively, while for tall structures, it is essential to employ dissipaters capable of controlling high deformations.

Finally, further research is recommended to explore variations in geometry, soil conditions, structural configurations, and the presence of irregularities, as well as the simultaneous combination of different types of devices, with the aim of further optimizing the seismic response of buildings. This approach would help broaden strategies for mitigating seismic vulnerability across a wide range of construction contexts.

REFERENCES

- BBC News Mundo, "Taiwan earthquake magnitude 7.4." Accessed: Jan. 28, 2025. [Online]. Available: https://www.bbc.com/mundo/articles/cx0zz4qwkxyo
- [2] BBC Mundo, "Ecuador earthquake magnitude 7.8." Accessed: Mar. 17, 2025. [Online]. Available: https://www.bbc.com/mundo/noticias/2016/04/160416_ec uador_terremoto_magnitud_colombia_peru_bm
- [3] C. Guadalupe, E. Alfredo, and R. Rotondaro, "Earthen Architecture in Seismic Zones: Latin America and the Pacific Fire Belt," Journal of Construction Research, vol. 3, no. 1, pp. 35–45, Sep. 2021, doi: 10.30564/JCR.V3I1.3263.
- [4] Juan Carlos Guzmán, "Lima carries a seismic silence of 278 years." Accessed: Mar. 17, 2025. [Online]. Available: https://andina.pe/agencia/noticia-lima-arrastra-silencio-sis mico-278-anos-y-no-esta-libre-temblor-fuerte-magnitud-8 57936.aspx
- [5] TvPe Noticias, "2007 earthquake in Pisco." Accessed: Mar. 17, 2025. [Online]. Available: https://www.tvperu.gob.pe/noticias/nacionales/terremoto-en-pisco-2007-17-anos-de-un-sismo-devastador
- [6] H. Tavera, "Analysis and evaluation of seismicity patterns and seismic scenarios on the western edge of Peru," Nov. 01, 2020, Instituto Geof sico del Perú Accessed: Mar. 17, 2025. [Online]. Available: http://hdl.handle.net/20.500.12816/48 93
- [7] B. J. Ayay Fernandez, "Structural design of an eighteen-story building and verification of seismic performance through a nonlinear static analysis," Jun. 2024, Accessed: Mar. 17, 2025. [Online]. Available: http://repositorio.unprg.edu.pe/handle/20.500.12893/13171
- [8] M. A. Quichimbo Vinces and E. D. Valdez Moreira, Structural performance analysis of a reinforced concrete structure with seismic dissipation systems, Undergraduate thesis, Universidad Politécnica Salesiana, Guayaquil, Ecuador, Jan. 2024.
- [9] D. Dominguez-Santos, "Optimization and analysis of

- hysteretic energy dissipators in reinforced concrete frame structures of five, 10 and 15 stories," International Journal of Protective Structures, Oct. 2024, doi: 10.1177/20414196241286157/SUPPL_FILE/SJ-PDF-1-PR S-10.1177 20414196241286157.PDF.
- [10] D. Noriega Silva, "Analysis and evaluation of a conventional model and a model with the integration of SLB seismic dampers of the Central Headquarters, an eight-story building plus a basement, at the Regional Government of Ucayali in the city of Pucallpa - Ucayali." Accessed: Mar. 17, 2025. [Online]. Available: https://repositorio.unu.edu.pe/items/28f2ebad-9f31-4baf-ae 32-3e847dc98ad9
- [11] H. Martin Hernandez Morales, H. Scaletti, H. H. Morales, L. B. Rotondo, and & H. S. Farina, "Simulating the hysteretic behavior of a SLB energy dissipation device via Unified Mechanics Theory," Jun. 2024. [Online]. Available: https://www.researchgate.net/publication/377722812
- [12] N. T. J. Luis, C. V. Neicer, M. C. R. Kevin, L. G. Eduardo, G. Q. D. Antonio, and L. A. López-Lau, "Performance Analysis of Energy Dissipators Implemented in Buildings," Jul. 19, 2023. Accessed: Mar. 17, 2025. [Online]. Available: https://research.upn.edu.pe/es/publications/an%C3%A1lisis-del-desempe%C3%B1o-de-disipadores-de-energ%C3%ADa-implementados-en
- [13] Y. Zhou, Y. Xiao, and M. Samier Sebaq, "Energy-based fragility curves of building structures equipped with viscous dampers," Structures, vol. 44, pp. 1660–1679, Oct. 2022, doi: 10.1016/J.ISTRUC.2022.08.101.
- [14] L. Guo, J. Wang, W. Wang, and H. Wang, "Performance-based seismic design and vulnerability assessment of concrete frame retrofitted by metallic dampers," Structures, vol. 57, p. 105073, Nov. 2023, doi: 10.1016/J.ISTRUC.2023.105073.
- [15] G. Xu et al., "Seismic resilience enhancement for building structures: A comprehensive review and outlook," Structures, vol. 59, p. 105738, Jan. 2024, doi: 10.1016/J.ISTRUC.2023.105738.
- [16] D. He, X. Cheng, H. Liu, Y. Li, H. Zhang, and Z. Ding, "Machine learning-based seismic fragility curves of regular infilled RC frames," Journal of Building Engineering, vol. 99, p. 111545, Apr. 2025, doi: 10.1016/J.JOBE.2024.1115 45.
- [17] J. Wang, J. Men, Q. Zhang, D. Fan, Z. Zhang, and C. H. Huang, "Seismic performance evaluation of a novel shape-optimized composite metallic yielding damper," Eng Struct, vol. 268, p. 114714, Oct. 2022, doi: 10.1016/J.ENGSTRUCT.2022.114714.
- [18] A. A. Youssef, M. R. Esfahani, and M. S. Zareian, "Experimental evaluation of post-tensioned hybrid coupled shear wall system with TADAS steel dampers at the beam-wall interface," Structures, vol. 53, pp. 1283–1299, Jul. 2023, doi: 10.1016/J.ISTRUC.2023.04.122.
- [19] K. Y. M. Almajhali, M. He, and W. Alhaddad, "Enhancing seismic performance of structures: A comprehensive review of hybrid passive energy dissipation devices," Structures, vol. 69, p. 107223, Nov. 2024, doi: 10.1016/J.ISTRUC.2024.107223.
- [20] H. Shojaeifar, A. Maleki, and M. A. Lotfollahi-Yaghin, "Performance Evaluation of Curved-TADAS Damper on

- Seismic Response of Moment Resisting Steel Frame," International Journal of Engineering, vol. 33, no. 1, pp. 55– 67, Jan. 2020, doi: 10.5829/IJE.2020.33.01A.07.
- [21] M. TahamouliRoudsari, K. Cheraghi, and R. Aghayari, "Investigating the Retrofit of RC Frames Using TADAS Yielding Dampers," SDHM Structural Durability and Health Monitoring, vol. 16, no. 4, pp. 343–359, Dec. 2022, doi: 10.32604/SDHM.2022.07927.
- [22] K. Cheraghi, M. TahamouliRoudsari, S. Kiasat, and K. Cheraghi, "Numerical study of metallic dampers' effect on seismic performance of concrete frames," Asian Journal of Civil Engineering, vol. 25, no. 3, pp. 2431–2441, Apr. 2024, doi: 10.1007/S42107-023-00917-6/METRICS.
- Houshmand-Sarvestani, A. Totonchi, M. "Numerical Shahmohammadi, and H. Salehipour, assessment of the effects of ADAS yielding metallic dampers on the structural behavior of steel shear walls (SSWs)," Mechanics Based Design of Structures and Machines, vol. 51, no. 3, pp. 1626-1644, 2023, doi: 10.1080/15397734.2021.1875328.
- [24] M. TahamouliRoudsari, M. B. Eslamimanesh, A. R. Entezari, O. Noori, and M. Torkaman, "Experimental Assessment of Retrofitting RC Moment Resisting Frames with ADAS and TADAS Yielding Dampers," Structures, vol. 14, pp. 75-87, Jun. 2018, doi: 10.1016/J.ISTRUC.201 8.02.005.
- [25] R. Siami Kaleybar and P. Tehrani, "Effects of using different arrangements and types of viscous dampers on seismic performance of intermediate steel moment frames in comparison with different passive dampers," Structures, 3382-3396. 33. pp. Oct. 10.1016/J.ISTRUC.2021.06.079.
- [26] S. Kiadarbandsari, M. Firoozi Nezamabadi, H. Abbasi, and F. Yaghoobi Vayeghan, "Analytical and experimental investigation of steel friction dampers and horizontal brake pads in chevron frames under cyclic loads," Structures, vol. 40, pp. 256-272, Jun. 2022, doi: 10.1016/J.ISTRUC.2022. 04.015.
- [27] N. B.K., R. K. C.M., V. R. D., N. B.K., R. K. C.M., and V. R. D., "Earthquakes and Structures," Earthquakes and Structures, vol. 10, no. 3, p. 629, 2018, doi: 10.12989/EAS.2016.10.3.629.
- [28] S. Rajkumari, K. Thakkar, and H. Goyal, "Fragility analysis of structures subjected to seismic excitation: A state-of-the-art review," Structures, vol. 40, pp. 303-316, Jun. 2022, doi: 10.1016/J.ISTRUC.2022.04.023.
- [29] N. K. Kothapalli, R. S. Chidambaram, and P. Agarwal, "Experimental Evaluation of Steel Bracings and Metallic Yield Damper as Retrofit Techniques for Severely Damaged RC Building Frames," Journal of Earthquake Engineering, vol. 27, no. 12, pp. 3564-3587, Sep. 2023, doi: 10.1080/13632469.2022.2141373.
- [30] M. D. Titirla, "A State-of-the-Art Review of Passive Energy Dissipation Systems in Steel Braces," Buildings 2023, Vol. 13, Page 851, vol. 13, no. 4, p. 851, Mar. 2023, doi: 10.3390/BUILDINGS13040851.
- [31] G. Bozzo Fernández, L. Perez, E. Miranda, J. M. Bairán Garc á, and L. M. Bozzo Rotondo, "Optimal set-up confirguation for testing stiff energy-dissipating devices under large displacements," WCEE 18: World Conference

- on Earthquake Engineering: online proceedings, pp. 1–12, 2024, Accessed: Mar. 18, 2025. [Online]. Available: https://upcommons.upc.edu/handle/2117/422548
- [32] T. S. Eom and H. G. Park, "Evaluation of energy dissipation of slender reinforced concrete members and its applications," Eng Struct, vol. 32, no. 9, pp. 2884-2893, Sep. 2018, doi: 10.1016/J.ENGSTRUCT.2010.05.007.
- [33] E. Saleh, "The development of fragility curves using calibrated probabilistic classifiers," Structures, vol. 64, p. 106618, Jun. 2024, doi: 10.1016/J.ISTRUC.2024.106618.
- [34] R. M. Bosse, J. Flórez-López, G. M. S. Gidrão, I. D. Rodrigues, and A. T. Beck, "Collapse mechanisms and fragility curves based on Lumped Damage Mechanics for RC frames subjected to earthquakes," Eng Struct, vol. 311, p. 118115, Jul. 2024, doi: 10.1016/J.ENGSTRUCT.2024.1 18115.
- [35] J. A. B. Tapia, R. A. T. Coloma, and D. P. G. Cuasapaz, "Structural Influence of SLB Dissipators for Decoupled Walls in Reinforced Concrete Structures and Bracing in Structures," Revista Técnica de la Facultad de Ingenier á Universidad del Zulia, vol. 45, no. 45, pp. 185-200, Sep. 2022, doi: 10.22209/RT.V45N3A05.
- [36] G. Smiroldo, M. Fasan, and C. Amadio, "Fragility curves for reinforced concrete frames characterised by different regularity," Procedia Structural Integrity, vol. 44, pp. 283-290, Jan. 2023, doi: 10.1016/J.PROSTR.2023.01.037.
- [37] E. Garavaglia, G. Angjeliu, and G. Cardani, "Simplified seismic vulnerability analysis of historic residential buildings with fragility curves," Procedia Structural Integrity, vol. 44, pp. 155-162, Jan. 2023, doi: 10.1016/J.PROSTR.2023.01.021.
- [38] M. Zucconi, F. Romano, and B. Ferracuti, "Typological fragility curves for RC buildings: influence of damage index and building sample selection," Eng Struct, vol. 266, p. 114627, Sep. 2022, doi: 10.1016/J.ENGSTRUCT.2022. 114627.
- [39] Reglamento Nacional de Edificaciones, "Standard E.030 Earthquake-Resistant Design," Gobierno del Per ú, pp. 1–81, 2020, Accessed: Mar. 18, 2025. [Online]. Available: https://drive.google.com/file/u/1/d/1W14N6JldWPN8wUZ SqWZnUphg6C559bi-/view?usp=embed_facebook
- [40] Reglamento Nacional de Edificaciones, "Standard E.020 Loads." Accessed: Mar. 18, 2025. [Online]. Available: https://drive.google.com/file/d/15atg-9w0OEXjR5C1m6IX UFihwYeUh1aN/view
- [41] Computers and Structures (CSI), "ETABS | BUILDING ANALYSIS AND DESIGN." Accessed: Mar. 18, 2025. [Online]. Available:https://www.csiamerica.com/products/ etabs
- [42] Reglamento Nacional de Edificaciones, "Standard E.060 Reinforced concrete." Accessed: Mar. 18, 2025. [Online]. Available: https://drive.google.com/file/d/19EYUVMgwv m6rDs47GV374avco2ylU5Kz/view
- [43] N. F. Ampuero Cardenas, "Structural design of a six-story reinforced concrete multi-family building located in Surquillo," May 08, 2024, Pontificia Universidad Católica del Perú Accessed: Mar. 18, 2025. [Online]. Available: http://hdl.handle.net/20.500.12404/27753

- [44] P. Jesus, Q. Cartolin, J. A. Muñoz, and P. Lima, "Earthquake-resistant design in reinforced concrete of a five-story building with a basement," Aug. 2024.
- [45] M. Flores and V. Ilich, "Reinforced concrete structural design of a 7-story multi-family building in the Los Olivos district, Lima," Jan. 15, 2025, Pontificia Universidad Católica del Perú Accessed: Mar. 18, 2025. [Online]. Available: http://hdl.handle.net/20.500.12404/29689
- [46] L. Bozzo and G. Gaxiola, "THE 'RIGID-FLEXIBLE-DUCTILE' CONCEPT AND SLB CONNECTIONS," Jan. 2018. Accessed: Mar. 18, 2025. [Online]. Available: https://www.academia.edu/30347209/ EL_CONCEPTO_RIGIDO_FLEXIBLE_DUCTIL_Y_LA S_CONEXIONES_SLB
- [47] F. Enciso Navarro, "Comparative analysis of the seismic design of a structure with continuous walls and with decoupled walls incorporating SLB dissipators in the city of Huancayo," Universidad Nacional del Centro del Perú, 2019, Accessed: Mar. 18, 2025. [Online]. Available: http://repositorio.uncp.edu.pe/handle/20.500.12894/5046
- [48] H. P. Jesús Paucarpura and H. P. Jesús Paucarpura, "Structural analysis and reinforcement of an irregular building with hysteretic dampers," Universidad Nacional de Ingenier á, 2019, Accessed: Mar. 18, 2025. [Online]. Available: https://repositorio.uni.edu.pe/handle/20.500.140 76/20247
- [49] R. Aguiar, M. Rodr guez, and D. Mora, "Seismic analysis of structures with ADAS or TADAS energy dissipators," Jan. 2018.
- [50] L. Bozzo, "SLB Devices Bozzo Shear Link Seismic Dissipators." Accessed: Mar. 18, 2025. [Online]. Available:

- https://slbdevices.com/
- [51] CISMID, "CISMID Japanese Peruvian Center for Seismic Research and Disaster Mitigation." Accessed: Mar. 18, 2025. [Online]. Available: https://www.cismid.uni.edu.pe/
- [52] Seismosoft Ltd, "SeismoSpect Signal Processing for Ground Motion Records - Seismosoft." Accessed: Mar. 18, 2025. [Online]. Available: https://seismosoft.com/products/seismospect/
- [53] F. Guerrero and J. López, "Correction of accelerographic records: filtering and baseline correction." Accessed: Mar. 18, 2025. [Online]. Available: https://smis.mx/index.php/R IS
- [54] T. Rossetto et al., "FRACAS: A capacity spectrum approach for seismic fragility assessment including record-to-record variability," Eng Struct, vol. 125, pp. 337– 348, Oct. 2016, doi: 10.1016/J.ENGSTRUCT.2016.06.043.
- [55] ACI Committee 318, 318-19 Building Code Requirements for Structural Concrete and Commentary. American Concrete Institute, 2019. doi: 10.14359/51716937.
- [56] A. M. Reinhorn and M. R. Willford, "Nonlinear Structural Analysis For Seismic Design A Guide for Practicing Engineers Gregory G. Deierlein," Oct. 2010. [Online]. Available: www.curee.org
- [57] American Society of Civil Engineers., Seismic evaluation and retrofit of existing buildings: ASCE/SEI, 41-17. American Society of Civil Engineers, 2017.
- [58] V. AMERICAN SOCIETY OF CIVIL ENGINEERS Reston, "FEDERAL EMERGENCY MANAGEMENT AGENCY FEMA 356 BUILDINGS," Nov. 2000. [Online]. Available: https://www.nehrp.gov/pdf/fema356.pdf